From Adsorption to Precipitation of U(VI): What is the Role of pH and Natural Organic Matter?

Carmen A. Velasco,

Department of Civil, Construction and Environmental Engineering, MSC01 1070, University of New Mexico, Albuquerque, New Mexico 87131, United States;

Adrian J. Brearley,

Department of Earth and Planetary Sciences, MSC03 2040, University of New Mexico, Albuquerque, New Mexico 87131, United States

Jorge Gonzalez-Estrella,

School of Civil and Environmental Engineering, Oklahoma State University, Stillwater, Oklahoma 74078, United States;

Abdul-Mehdi S. Ali,

Department of Earth and Planetary Sciences, MSC03 2040, University of New Mexico, Albuquerque, New Mexico 87131, United States

María Isabel Meza,

Department of Civil, Construction and Environmental Engineering, MSC01 1070, University of New Mexico, Albuquerque, New Mexico 87131, United States

Stephen E. Cabaniss,

Department of Chemistry and Chemical Biology, University of New Mexico, Albuquerque, New Mexico 87131, United States

Bruce M. Thomson,

Department of Civil, Construction and Environmental Engineering, MSC01 1070, University of New Mexico, Albuquerque, New Mexico 87131, United States

Tori Z. Forbes,

Department of Chemistry, University of Iowa, Iowa City, Iowa 52242, United States;

Juan S. Lezama Pacheco,

Corresponding Authors: Carmen A. Velasco – Department of Civil, Construction and Environmental Engineering, MSC01 1070, University of New Mexico, Albuquerque, New Mexico 87131, United States; cavelasco@unm.edu, **José M. Cerrato** – Department of Civil, Construction and Environmental Engineering, MSC01 1070, University of New Mexico, Albuquerque, New Mexico 87131, United States; Phone: (001) (505) 277-0870; jcerrato@unm.edu; Fax: (001) (505) 277-1918.

Department of Earth System Science, Stanford University, Stanford, California 94305, United States

José M. Cerrato

Department of Civil, Construction and Environmental Engineering, MSC01 1070, University of New Mexico, Albuquerque, New Mexico 87131, United States;

Abstract

We investigated interfacial reactions of U(VI) in the presence of Suwannee River natural organic matter (NOM) at acidic and neutral pH. Laboratory batch experiments show that the adsorption and precipitation of U(VI) in the presence of NOM occur at pH 2 and pH 4, while the aqueous complexation of U by dissolved organic matter is favored at pH 7, preventing its precipitation. Spectroscopic analyses indicate that U(VI) is mainly adsorbed to the particulate organic matter at pH 4. However, U(VI)-bearing ultrafine to nanocrystalline solids were identified at pH 4 by electron microscopy. This study shows the promotion of U(VI) precipitation by NOM at low pH which may be relevant to the formation of mineralized deposits, radioactive waste repositories, wetlands, and other U- and organic-rich environmental systems.

Graphical Abstract
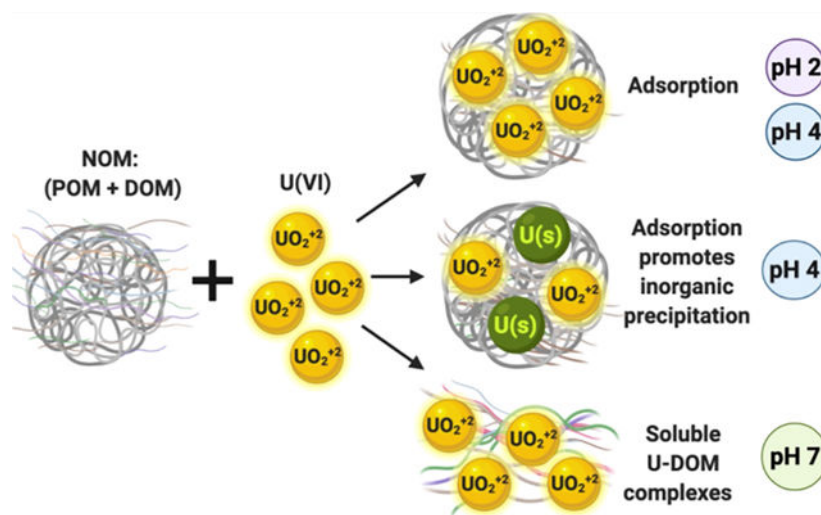
Keywords

microscopy; spectroscopy; uranium; natural organic matter; humate; complexation; precipitation

INTRODUCTION

The toxic effects of uranium (U) are well known[1,2] and present a threat to communities with elevated concentrations in waters and soils. A recent study found that carbon-rich, U-bearing particulates increase U toxicity in comparison to water-soluble U ions.[3] U frequently co-occurs in geologic deposits with natural organic matter (NOM); for example, NOM abundance ranges from 1 to 57% in Eocene sandstone and U-mineralized deposits.[4–6] In

oxidizing environments, the most common oxidation state is U(VI), which forms complexes with inorganic (OH^-, SO_4^{2-}, CO_3^{2-}, and PO_4^{3-}) and organic ligands. Seasonal variations in pH and NOM concentrations could influence the variability of U(VI) concentrations in surface waters and the accumulation of U in riparian soils and plants.[7,8] Yet, interactions of U and NOM affecting U solubility and transport in surface oxidizing environments remain poorly understood.

NOM is a heterogeneous mixture of organic molecules, often characterized by bulk or macroscopic properties such as molecular weight, the ratio of C–H–O–N, aqueous solubility, and partitioning into organic solvents. Dissolved OM (DOM) is operationally defined as the organic matter fraction that passes through a 0.45 μm filter, particulate OM (POM) refers to the organic matter retained by a 0.45 μm filter, and colloids are the fraction that passes through a 0.2 μm filter.[9–11] At high pH values,[10,12] the deprotonation of organic functional groups (e.g., amine, phenolic, and carboxylic groups) increases the average negative charge and solubility of NOM, while metal cation complexation at low pH neutralizes the charge and decreases the solubility.[12–14] The solubility of NOM, in turn, influences the complexation, sorption, and transport of metals, including U.[15]

The pH-dependent solubility of U(VI) in oxidizing environments is also affected by the complexation with organic ligands. For example, at low pH, U forms bidentate surface complexes with NOM carboxylate groups.[16] Adsorption of UO_2^{2+} onto solid NOM has been demonstrated in the pH range of 4–6, in which aqueous U-humate complexes are also predominant.[17,18] More specifically, DOM can form soluble complexes with U, whereas POM removes U from solution through adsorption reactions.[19–21]

A detailed understanding on the mechanism and controls that pH exerts on the precipitation/adsorption of U in the presence of NOM is sorely lacking. The stability of reduced U after reaction with NOM has been studied by previous studies.[6,22,23] However, our understanding about the solubility of uranium after reaction with NOM remains limited. Cumberland et al.,[24] noted the importance of NOM in the fate and transport of U in the environment and identified the following unresolved and critical questions that must be answered to advance our understanding of uranium mobility:

1. How are U(VI) solubilization and transport affected by the processes of precipitation of inorganic U phases, DOM complexation, and the precipitation/sorption of NOM accompanied by co-precipitation/adsorption of U?

2. How and under what environmental conditions can U(VI) solubilization by complexation with NOM outweigh the removal of U(VI) from solution by NOM-related precipitation/adsorption processes?

3. How stable or labile are U(VI) surface or solid species created in the presence of NOM?

The pursuit of these questions justifies the need for this study.

The objective of this work was to identify the effect of pH on the adsorption, precipitation, and solubilization of U(VI) in the presence of NOM. This investigation focused on U(VI),

the oxidation state that is thermodynamically stable in most surface waters. The novelty of this investigation is the identification of the precipitation products formed after the reaction of U(VI) with NOM by transmission electron microscopy (TEM) and X-ray absorption spectroscopy (XAS) and other advanced electron microscopy and spectroscopy techniques. The results of our study advance our understanding of precipitation reactions which affect the solubility of U(VI) and NOM in natural and anthropogenic water systems at acidic and circumneutral pH.

MATERIALS AND METHODS

Chemicals.

Suwannee River (SR) NOM was purchased from the International Humic Substance Society (IHSS catalogue number 1R101N). We used the SRNOM in our study because it is well characterized, commercially available, and a reference material. U in 4% HNO_3 for an analytical grade standard was acquired from SCP Science, Plasma Cal. Potassium chloride (KCl) 99.999% trace metal basis was purchased from Sigma-Aldrich. We used 10 N NaOH solution from EMD and 2% HNO_3 PlasmaPure grade from SCP Science to adjust the pH.

Batch Experiments.

In this paper, we use U to denote U(VI) unless otherwise stated. We conducted 50 mL batch experiments at pH 2, pH 4, and pH 7 to assess the effect of pH on U and NOM precipitation. The variation of pH throughout the experiment was <0.1 log unit. The U and NOM concentrations chosen for this study are based on conditions reported in a previous investigation using solid samples from the Jackpile Mine, New Mexico, USA.[5] In this study, we used controlled experimental conditions to work in a more constrained system (i.e., SRNOM and uranyl nitrate) to reduce the complexity of working with natural samples and enable specific reactions between U and NOM to be studied.[5] We were interested in rapid reactions (<24 h) between U and NOM which are relevant for certain natural and engineered systems. Thus, we chose reaction times of 0.5 and 24 h for our experiments. Ionic strength can have a significant effect on cation binding to NOM at near neutral pH and can influence cation adsorption to organic functional groups. We therefore used 0.010 M KCl as a swamping electrolyte for controlled ionic strength conditions in the experiments.

Two stock solutions of 400 mg L^{-1} NOM and 200 μM-$UO_2(NO_3)_2$ in 0.02 M KCl were prepared. Equal volumes of stock solutions were added to 50 mL polypropylene centrifuge tubes to reach an initial concentration of 200 mg L^{-1} NOM and 100 μM $UO_2(NO_3)_2$ in 0.01 M KCl, as shown in Table S1. Control experiments containing only 100 μM $UO_2(NO_3)_2$ in 0.01 M KCl (control U) and only 200 mg L^{-1} NOM (control NOM) were prepared as well. We conducted six replicates of each experiment. pH adjustments were conducted with HNO_3 or NaOH. Experiments were then capped and placed in a tumbler. One additional control experiment in the absence of KCl and NaOH was conducted to identify the effect of KCl and NaOH on interfacial reactions between U and NOM at the longest reaction time (24 h). We used NH_4OH to adjust the pH. This sample was named control 1; solids collected from this reaction were analyzed by TEM and XAS.

Aqueous Analyses.

Chemical analyses were conducted on supernatant samples collected from all experiments after the reaction time (0.5 and 24 h). Samples were centrifuged, and the supernatant was filtered through 0.20 μm membrane filters (Pall Acrodisc, Westborough, MA, USA). Samples were acidified using ultrapure HNO_3 for subsequent measurement of the soluble U concentration by inductively coupled plasma mass spectrometry.

Dissolved organic carbon (DOC) measurements were conducted according to Standard Methods 5310c using the persulfate-ultraviolet method using a Teledyne-Tekmar Fusion TOC analyzer. All samples were filtered through a 0.20 μm membrane filter to remove colloidal fractions and only quantify the fraction that passed through this filter which we are referring as DOM fraction. An auto dilution of 10 to 1 for all samples was performed and analyzed by a Fusion TOC analyzer. The carbon content in the NOM used in this study was 50.7 wt % according to the IHSS catalogue, so that a solution of 200 mg/L of NOM corresponds to 101.4 mg L^{-1} of DOC.

We measured the zeta (ζ)-potential of unfiltered samples from experiments U–KCl-NOM, control U, and control NOM after centrifugation and filtration using a Malvern Zetasizer Nano-ZS equipped with a He–Ne laser (633 nm) and noninvasive backscatter optics. The ζ-potential in each sample was measured three times and the average was calculated.

Statistical analyses were conducted to analyze soluble U and DOC data using R statistical software. The Shapiro–Wilks normality test was used to determine if the data were parametric or nonparametric (Table S3). A three-way Anova was used for multivariant analyses as a function of pH (2, 4, and 7), considering concentrations of U and DOC in control experiment U, experiment U-NOM, and time (0.5 and 24 h). A t-test was also used to assess the significance of differences between U and U–NOM at each pH value tested in our experiments.

Solid Analyses.

Solids were collected by centrifuging samples after the corresponding reaction time. Solids from triplicate experiments were combined to increase the homogeneity and available mass for analyses. Samples were air-dried and stored in Eppendorf Safe-Lock microcentrifuge tubes at room temperature until analyzed. Solid analyses were conducted within 2–4 weeks since samples were collected to prevent any changes due to the storage time. Solid samples were analyzed by the following methods.

X-ray Fluorescence.—Bulk chemical analysis to determine the elemental composition of precipitates was done using an EDAX Orbis μ-XRF spectrometer with a Rh anode X-ray tube. It was operated at 40 kV and 800 μA with the 30 μm polycapillary optic. The samples were evacuated to 0.3 Torr, and data were collected for 600 live seconds. We measured five analytical points on each sample, and we present the average of all measurements.

Electron Microprobe Microanalysis X-ray Mapping.—We conducted electron microprobe microanalysis (EPMA) on solid samples collected from experiment U–KCl-NOM after 0.5 h of reaction to confirm the presence of U on these samples. We chose

these samples because soluble U concentration decreased after 0.5 h. A droplet of the disaggregated sample suspended in acetone was deposited on a silicon wafer and on 3 mm Cu mesh grids covered with a holey carbon support film for TEM analysis. Samples mounted on the silicon wafer for EPMA were coated with approximately 150 nm of gold to enable the quantitative determination of carbon. Qualitative X-ray mapping was performed on a JEOL 8200 Superprobe electron microprobe using wavelength-dispersive spectrometry (WDS). Operating conditions were 15 kV accelerating voltage, 30 nA beam current, and a beam diameter of 1 μm. Qualitative WDS mapping was also conducted on the TEM grids to locate U-rich particles prior to TEM analysis.

Transmission Electron Microscopy and Electron Energy Loss Spectroscopy. —TEM was conducted using bright-field TEM imaging (BFTEM), high-angle annular dark-field scanning TEM (STEM) imaging, selected area electron diffraction (SAED), and energy-dispersive X-ray spectroscopy (EDS) using a JEOL 2010F field emission gun scanning transmission electron microscope instrument operating at 200 kV. Electron energy loss spectroscopy (EELS) was carried out on the JEOL 2010F using GATAN GIF 2000 image filtering system, and EDS X-ray analysis was performed using an Oxford AZTec EDS system with an ultrathin window XMax 80N 80 mm^2 SDD EDS detector. Both point EDS analysis in the TEM mode and X-ray maps in the STEM mode were obtained. Quantification of EDS data was carried out using the thin-film approximation using theoretical K-factors. TEM analyses were conducted on solids collected from experiment U–KCl-NOM, control U (U + KCl), and control NOM (NOM). Table S1 summarizes these analyses. Additional information about the identification of solids phases by electron diffraction is available in the Supporting Information.

EELS was carried out on a sample collected after 24 h from experiment U–KCl-NOM at pH 4 to investigate the composition of the crystalline solids. The EELS measurements on the solids were carried out using the GATAN GIF system at 197 kV in the imaging mode on the carbon edge with an energy resolution of 1 eV. Calibration of each spectrum was carried out using the C K edge at 284 eV and the K L_2 edge at 296 eV.

X-ray Absorption Spectroscopy.—XAS measurements were conducted on solids collected from experiments of U–KCl-NOM and U–NOM (control 1) at pH 4 after 24 h reaction time. We chose these samples because they showed the most prominent decrease in the soluble U concentration of the solution at pH 4 and to evaluate the effect of KCl on the reactions of U and NOM at pH 4. XAS measurements were conducted on beamline 7–3 at the Stanford Synchrotron Radiation Lightsource (SSRL) at the U L_{III} edge in the fluorescence mode, and we used a 32-element germanium fluorescence detector. We collected data for the X-ray absorption near-edge structure (XANES) and the extended X-ray absorption fine structure (EXAFS) spectra. Measurements were conducted at 10 K using a closed cycle cryostat in a helium atmosphere. Samples were pulverized and pressed into the slots of aluminum holders and sealed with Kapton tape on both sides. Data processing and analyses for XAS were conducted using Athena and Artemis software.[25]

RESULTS

Effect of NOM on U Solubility.

Experiments at pH 2.—The soluble U concentration decreased in U–KCl-NOM experiments after 0.5 h from an initial concentration (100 μM), but then resolubilized after 24 h. The soluble U concentration was 78.5 ± 10.8 μM after 0.5 h and increased to 99.2 ± 3.7 μM after 24 h. In control experiments without NOM (control U), soluble U concentration remained constant at 100.5 ± 0.21 μM for the duration of the experiment (Figure 1). In U–KCl-NOM experiments, DOC was 83.1 ± 2.7 mg L^{-1} after 0.5 h, 82.6 ± 2.2 mg L^{-1} after 24 h, and in control experiments without U (control NOM), DOC was 85.2 ± 0.01 mg L^{-1} (Figure S1).

Experiments at pH 4.—U was less soluble at pH 4 than at pH 2 after 0.5 h after reaction with NOM. Soluble U concentration increased after 24 h relative to 0.5 h, as observed in experiments conducted at pH 2. Soluble U concentration was 62.6 ± 19.7 μM after 0.5 h and increased to 95.3 ± 3.1 μM after 24 h in U–KCl-NOM experiments, likely due to the desorption of U. There was little change in the soluble U concentration in control U experiments at 0.5 and 24 h (Figure 1). In U–KCl-NOM experiments, DOC was 86.6 ± 1.3 mg L^{-1} after 0.5 h and 85.1 ± 0.8 mg L^{-1} after 24 h. In experiments without U (control NOM), DOC was 86.6 ± 0.06 mg L^{-1} (Figure S1).

Experiments at pH 7.—In U–KCl-NOM experiments at pH 7, the soluble U concentrations remained close to the initial concentration (100 μM) over time. These results suggest that the aqueous complexation of U by DOM increases the solubility of U at pH 7 relative to the experiments conducted without NOM. The soluble U concentration was 87.4 ± 3.3 μM after 0.5 h and 99.6 ± 3.7 μM after 24 h (Figure 1). Our observation of increased solubility is consistent with another study which reported that the complexation of U by organic ligands at circumneutral pH increases the mobility of aqueous U species.[26] The DOC concentrations measured in U–KCl-NOM experiments at pH 7 were slightly higher than those measured at pH 2 and pH 4. In U–KCl-NOM experiments at pH 7, the DOC concentration was 87.7 ± 0.4 mg L^{-1} after 0.5 h and 88.6 ± 0.1 mg L^{-1} after 24 h. In experiments without U (control NOM) at pH 7, the DOC concentration was 89.1 ± 0.01 mg L^{-1} (Figure S1). In the absence of NOM (U control experiment), the soluble U concentration decreased over time due to inorganic precipitation at pH 7. The soluble U concentration for the U control experiment was 37.3 ± 13.1 μM after 0.5 h and 1.8 ± 0.7 μM after 24 h compared to the initial concentration (100 μM). Advanced electron microscopic analyses of the precipitates from these experiments are described in the next subsection.

Statistical analyses indicate that our concentration data are normally distributed (p-values > 0.05 for normality tests). Three-way parametric Anova tests indicate statistical differences in soluble U concentrations for pH 2 and pH 4 with respect to time (0.5 and 24 h) and in U–KCl-NOM experiments (p-values <0.05). Statistical differences were also detected for pH 2, pH 4, and pH 7 with respect to control U experiments ($p < 0.05$). The DOC concentration for pH 2, pH 4, and pH 7 with respect to NOM control and U–KCl-NOM experiments were also statistically different (p-value < 0.05). There are no statistically significant differences

in the DOC concentration at pH 2, pH 4, and pH 7 with respect to time (p-value > 0.05, see Tables S3 and S4).

We measured the zeta (ζ)-potential of particulates in unfiltered samples from U–KCl-NOM experiments at pH 2 and pH 4. We focused on samples at pH 2 and pH 4 which contained precipitates, whereas no precipitation occurred at pH 7. ζ-potential measurements showed more negative surface charge density at pH 4 than at pH 2, as shown in Figure S2. For example, the ζ-potential of samples from experiments U–KCl-NOM conducted at pH 2 was −12.43 mV after 0.5 h and −13.40 mV after 24 h, while at pH 4 was −18.52 mV after 0.5 h and −19.41 mV after 24 h. The ζ-potential of precipitates in NOM control experiments at pH 2 was −14.68 after 0.5 h and −13.24 after 24 h, while at pH 4 was −31.09 mV after 0.5 h and −29.99 mV after 24 h. The ζ-potential in U control experiments was close to zero at pH 2 (1.66 mV after 0.5 h and 0.98 mV after 24 h) and pH 4 (−0.61 mV after 0.5 h and −0.20 mV after 24 h). Even at pH 2 the dominant surface charge was negative, allowing for electrostatic attraction with positive uranyl (UO_2^{2+}) cations. ζ-potential of solid samples from the NOM control experiment was more negative compared to samples from the U–KCl-NOM experiment. These results suggest that the adsorption of uranyl cations onto POM occurred consistent with observations reported in other studies.[27,28]

Adsorbed and Precipitated Phases in Reacted Solids.

Micro X-ray Fluorescence.—Analysis by μ-XRF detected higher U concentrations on solids collected from experiments U–KCl-NOM at pH 4 (0.26 ± 0.05 atomic U % at 0.5 h and 0.20 ± 0.04 atomic U % at 24 h) compared to solids collected at pH 2 (0.09 ± 0.02 atomic U % at 0.5 h and 0.05 ± 0.01 U at 24 h, Figure S3). No solids were recovered from experiments U–KCl-NOM at pH 7. The highest measured concentration of U in solids from this study was from the U control experiments (no NOM) at pH 7 (2.30 ± 0.09 atomic U % at 0.5 h and 3.97 ± 0.38 atomic U % at 24 h). These results are consistent with the observations from analyses of soluble U concentration discussed earlier.

Analysis by μ-XRF also detected higher concentrations of K on solids collected from experiments U–KCl-NOM at pH 4 (6.90 ± 2.52 atomic K % at 0.5 h and 7.58 ± 2.28 atomic K % at 24 h) compared to solids collected at pH 2 (5.05 ± 2.92 atomic K % at 0.5 h and 2.99 ± 0.31 K at 24 h, Figure S3). The highest concentration of K detected was on solids collected from the control experiment containing only U and KCl at pH 7 (27.22 ± 0.61 atomic K % at 0.5 h and 27.39 ± 7.86 atomic K % at 24 h). The μ-XRF measurements we report represent the mass fraction of U and K in the solid but without accounting for the mass of C or O.

X-ray Absorption Spectroscopy.—We observed the maximum decrease in the soluble U concentration in U–KCl-NOM experiments at pH 4. The maximum U fraction on the solids analyzed by μ-XRF also corresponds to U–KCl-NOM experiments at pH 4. Thus, we chose the precipitates from reactions of U–KCl-NOM and U-NOM at pH 4 after 24 h to conduct XAS analyses. Note that XAS is a bulk, not a surface technique. Thus, these XAS analyses generate information about U associated with POM in the bulk solid. The main oxidation state of U in both samples was U(VI), evidenced by the presence of the

-yl shoulder and the energy at the inflection point as observed in the XANES spectra (Figure S4). Results from the EXAFS analyses showed that the U–O axial distances are 1.78 ± 0.01 for U-NOM and U–KCl-NOM. The distances between U–O equatorial pairs were 2.27 ± 0.04 and 2.43 ± 0.03 Å for both reactors at pH 4. We also found that U is mainly associated with POM on both samples, U is likely bound to carboxylic functional groups adsorbed to POM (Figure 2). We compared the reduced χ^2 and the best fit was obtained with seven-coordinate U–O equatorial pairs for the solids collected from reaction of U-NOM. Similarly, the best fit was obtained with six- or seven-coordinate U–O equatorial pairs for the solids collected after the reaction of U–KCl-NOM (Table S2). We identified distances of U–C pairs between 2.90 ± 0.03 and 3.44 ± 0.03 Å in samples from experiments U–KCl-NOM and U-NOM. We also identified a distance of 3.94 ± 0.03 Å between U–U pairs possibly due to the presence of crystalline or poorly crystalline phases in the sample.

Analyses by Electron Microscopy.—The adsorption of U onto amorphous POM was detected on solids collected from reactions of U–KCl-NOM at pH 2. Crystalline U–K phases associated with POM were detected at pH 4. U–K-bearing solid phases were detected at pH 7 in the absence of NOM (control U).

Experiment at pH 2.—In samples collected from reactions of U–KCl-NOM, we found no evidence of distinct U-bearing particles on the POM, although U was detected on POM after 0.5 and 24 h. WDS EPMA X-ray maps showed the spatial association of U and carbon (C) from POM after 0.5 h, likely due to the adsorption of U onto POM (Figure S5). U-bearing crystalline solids were not detected by TEM in samples at 0.5 and 24 h. The heterogeneous U concentration within the POM observed at 0.5 and 24 h and the absence of U-bearing particles suggest U is adsorbed onto POM at pH 2 (Figure 3). Analyses by TEM and STEM EDS mapping did not detect any U-rich particles either crystalline or amorphous at pH 2 (Figures 3C and S6). The DF-STEM images illustrate that high-Z nanoparticles are present associated with the POM at pH 2 (Figure S7) but appear to contain silicon rather than U (Figure 3B).

Experiments at pH 4.—The heterogeneous distribution of U in solids collected from reaction of U–KCl-NOM at pH 4 indicated the precipitation of U–Na–K-bearing crystalline phases in addition to the adsorption of U onto POM. The presence of U associated with both amorphous and crystalline solids on these samples contrasts with the observations at pH 2 where no crystalline solids were identified. The EPMA X-ray mapping of solids at pH 4 collected after 0.5 h showed less spatial association of U and C from POM compared to the samples at pH 2, likely because there is a lower concentration of POM at pH 2 than at pH 4 (Figure S5). Dark-field (DF)-STEM conducted on the solids collected from U–KCl-NOM precipitation after 0.5 h detected amorphous carbon-rich solids, which we infer is POM (Figure S7). BFTEM detected amorphous solids and U–K and U–Na crystalline particles (<0.5 μm) on the sample collected at 24 h. Heterogeneous composition was detected by TEM–EDS on amorphous and crystal solids; amorphous solids had lower U and K concentrations compared to the crystalline solids (Figure 3). STEM–EDS X-ray maps for solids collected from precipitation experiments in batch solutions of U–KCl-NOM after 24 at pH 4 indicate the association of U, C, Cl, Na, and K in these solids. U- and

K-rich particles were detected in this sample (Figure S8), and several possible phases could be present (e.g., grimselite, schoepite, compreignacite, and clarkeite). However, based on the *d*-spacings, angles between diffraction vectors, and the ratios of the diffraction vectors measured from SAED patterns, we determined that the crystalline solids are consistent with grimselite [$K_3NaUO_2(CO_3)_3 \cdot H_2O$] (Figure 3). There are no possible fits for the other three phases based on a search of all possible zone axes. Details of the identification of this phase are presented in the Supporting Information and Table S5. EELS spectra obtained from several individual crystals confirm that the phase is a carbonate, as shown in Figure 4.

Experiments at pH 7.—No precipitates were recovered from the U–KCl-NOM experiments at pH 7 after 0.5 or 24 h. However, we detected the inorganic precipitation of U- and K-bearing crystalline precipitates in the U control experiment by TEM (i.e., no NOM) at pH 7 (Figure S9). These solids exhibit stable crystalline structures. The composition and electron diffraction data are similar to clarkeite [$Na(UO_2)O(OH)(H_2O)_{0-1}$], but given the composition of the solution used for the experiments, the solid could contain K instead of Na in a similar mineral form to compreignacite [$K_2(UO_2)_6O_4(OH)(H_2O)_7$].[29,30]

DISCUSSION

Effect of NOM on U Solubility as a Function of pH.

Our results show that the soluble U concentration in the presence of NOM is affected by pH and reaction time. Several experimental and modeling studies reported the effect of humic acid (HA) and fulvic acid on U mobility through adsorption and complexation.[13,14,24,31] However, there are limited studies reporting adsorption and desorption of U onto NOM.[24,32] The adsorption of U–humic complexes onto quartz was enhanced between pH 3 and 6.[20] The soluble U concentration reported in this study likely decreased after 0.5 h by the adsorption of uranyl ions onto the POM. Consistent with our results, the adsorption of U onto other minerals and sediments has been observed to take place within 0.5 h.[33,34] For instance, rapid adsorption of U onto ferrihydrite, independent of pH, has been observed within minutes of the reaction.[35] The soluble U concentration likely increased after 24 h by U desorption reactions. A study using soils containing HA showed rapid desorption of U, whereas no desorption of U occurs in soils without HA.[36]

As pH increases from pH 2 to pH 7, NOM becomes more soluble due to the deprotonation of carboxyl functional groups. The high DOC concentration detected at pH 7 is consistent with another study reporting HA precipitation at low pH, while HA is soluble at high pH.[10] Our results agree with the literature showing that high DOC concentrations increase the solubility and mobility of U, especially when colloids are present.[20,24,37–39] Consistent with our findings, a previous study showed that higher pH promotes the dissolution of POM and increases the dissolved concentration of heavy metals through the formation of metal–organic complexes.[40] The aqueous complexation of dissolved humic substances with U at circumneutral pH can lead to less U adsorption onto POM. Specifically, the formation of U–HA aqueous complexes at neutral pH decreases U adsorption onto POM.[41]

Precipitates were observed in experiments with no NOM at pH 7. Other studies have shown that U(VI) precipitation can take place at pH > 4.[42,43] The precipitation of uranyl oxide hydrate phases {e.g., metaschoepite [$UO_3(H_2O)_2$], compreignacite [$K_2(UO_2)_6O_4(OH)_6(H_2O)_7$], sodium compreignacite [$Na_2(UO_2)_6O_4(OH)_6(H_2O)_7$], and clarkeite [$Na(UO_2)$-$O(OH)$] can occur at pH 5 to pH 7}.[29,30,34,44–46] The solubility of these solids depends on the concentration of U, other cations, and solution pH.[29,30,47,48]

From Adsorption to Precipitation.

The EXAFS analyses conducted in this study indicate that U is mainly adsorbed onto NOM. The shortest U–O distances occur at 1.78(1) Å ($N = 2$) that corresponds to the uranyl oxo moiety. Additional U–O distances of 2.27(4) and 2.43(2) Å correspond to typical coordination distances around the equatorial plane of the uranyl cation.

Our results agree with the findings from Denecke et al., which identified distances of 2.36 ± 0.05 and 2.48 ± 0.05 Å for a U–O distance for a bridging hydroxide group and bidentate coordination for the carboxylate groups associated with the surface of the HA.[49] The U–C interatomic distances we present herein are similar to the range reported by Regenspurg et al., which suggests that U–C distances can vary between 2.8 and 3.2 Å for synthetic uranyl compounds containing carboxylate groups.[50] Additional studies on U(VI) in the presence of organic matter also observed U–C distances of 2.9 Å, and Dublet et al. noted a distance at 3.4 Å, which they attributed to a uranyl humate complex.[38,39,51,52] The signatures corresponding to U–C interatomic distances observed in our study are also similar to those from U bound to biomass and cell walls,[19,23,39,52–56] again providing evidence that U is bound to organic C by surface complexation.

The TEM analyses integrated with SAED patterns suggest that in addition to the adsorbed U identified by EXAFS analyses, a crystalline phase consistent with grimselite is also present in solids obtained at pH 4. Carbonates have a very distinct sharp peak at 290 eV; however, the K L_2 edge in the EELS spectra occurs at 296 eV, resulting in a significant peak overlap between the K edge and C edge for carbonate. Nevertheless, a distinct shoulder at ~289 eV is apparent on the lower energy side of the K edge, about 1 eV lower than the typical energy of the carbonate peak in most minerals that occurs at 290.2 eV.[57] One possibility is that the energy of the carbonate peak is shifted to slightly lower energy in grimselite, as occurs, for example, in cerussite ($PbCO_3$), where the carbonate peak energy is 289.9 eV, but the energy shift is significantly larger in the case of grimselite. We also evaluated the possibility that this 289 eV shoulder is due to the presence of carboxylate groups coordinated to U, instead of carbonate. Such structures have been reported where U(VI) could be coordinated with other tricarboxylates[58] but retain the hexagonal symmetry of grimselite. However, such structures result in a much larger unit cell, which is inconsistent with our electron diffraction data. We therefore favor the interpretation that this peak is a carbonate peak, rather than the result of carboxylate.

Past studies have shown that grimselite forms under near-neutral to alkaline conditions and not at low pH,[59,60] suggesting that grimselite may be a metastable precipitate in these experiments. Another investigation reported the formation of metaschoepite [$UO_3(H_2O)_2$] at pH 4.2–4.3 and Na-compreignacite [$Na_2(UO_2)_6O_4(OH)_6\cdot7H_2O$] at pH ~5.[30] However,

the SAED patterns we found in our study do not coincide with metaschoepite or Na-compreignacite, and the presence of K in the EDS and EELS data is inconsistent with either of these phases. Thus, the solid precipitated from experiment U-KCL-NOM at pH 4 likely corresponds to a different U-bearing phase. TEM–EDS analyses of samples collected from the experiment of U-NOM in the absence of KCl at pH 4 after 24 h did not detect crystalline U-bearing solids. These results confirm that U is adsorbed to POM at pH 4 in the absence of KCl, in agreement with XAS results.

Grimselite [$K_3NaUO_2(CO_3)_3 \cdot H_2O$] precipitation at pH 4 is not predicted by chemical equilibrium analyses because the concentration of CO_3^{2-} ions in solution is negligible under acidic conditions as dictated by the speciation of dissolved inorganic carbon controlled by acid–base reactions. Thus, an alternative explanation for grimselite formation is that photocatalytic degradation of the NOM occurs in the solid state under these conditions, which results in the formation of an inorganic carbonate. DOM can undergo bleaching (destruction of chromophores) or mineralization (production of dissolved inorganic carbon) in the presence of UV light.[61] Mineralization can be influenced by various catalysts, with iron processes being the most well studied.[62] In this case, Fe(III) reduction occurring through the oxidation of DOM followed by reoxidation by dioxygen species. More recent literature has demonstrated that U(VI) can engage in a similar photocatalytic process under ambient light conditions where photoexcitation of U(VI) results in hydrogen abstraction from an organic substrate and reduces the metal center to the pentavalent state.[63,64] Additional interactions with O_2 gas result in reoxidation of U and formation of reactive dioxygen species in solution. The dioxygen radicals can invoke further mineralization processes and have previously been shown by Kravchuk and Forbes to degrade phosphonate molecules to the inorganic phosphate by breaking a C–P bond.[65] In addition, Kravchuk et al. also demonstrated that U(VI) can stabilize superoxide radicals and promote carbonation processes that specifically resulted in the formation of uranyl peroxide carbonate complexes and the grimselite phase through a solid-state transformation.[66] Both Kravchuk et al. and Blanes Díaz et al. also noted that photochemical degradation of U(VI) organic materials can take place in the solid state, and so these mineralization reactions may indeed occur following adsorption to the POM phase.[67]

In experiments at pH 7 in the absence of NOM, we identified a U(VI) solid phase. Thermodynamic modeling shows that schoepite [$(UO_2)_8O_2(OH)_{12} \cdot 12(H_2O)$] would be stable under these conditions.[30] Other studies conducted with goethite report U surface precipitation of crystalline uranyl precipitates (e.g., schoepite or metaschoepite) at pH 6[34] and at circumneutral pH.[24] However, the SAED data obtained for this sample in our study are not consistent with either schoepite or metaschoepite, but are most consistent with clarkeite [$Na-(UO_2)O(OH)$] nanocrystals, but possibly with another U-bearing phase that remains unidentified (Figure S9).

Mechanistic Insights.

This study shows the effect of pH on U(VI) adsorption, precipitation, and solubility in the presence of NOM. The EXAFS and TEM analyses indicate that U is primarily associated with POM at pH 2 and pH 4 due to adsorption. However, precipitation of crystalline

U-bearing phases was also detected in solids from reactions with NOM in a KCl solution at pH 4. These observations indicate that POM serves as a substrate for the adsorption and precipitation of U at pH 4. The interfacial reactions between U, KCl, and NOM at pH 7 show that the complexation of U–KCl-DOM increases the solubility of U at circumneutral pH.

We found differences in the adsorption and precipitation of U at 0.5 and 24 h in the presence of NOM at pH 4. The TEM data indicate heterogeneous distribution of amorphous and crystalline U-phases onto POM in samples collected after 0.5 and 24 h, suggesting that precipitation occurred as the reaction time reaches 24 h. Precipitates formed in solutions containing U, KCl, and NOM. Within the first 0.5 h of reaction, U is initially sorbed onto fine particles of POM which subsequently aggregate into larger POM flocs. Our findings suggest that at 0.5 h, the adsorption of U onto POM is the primary reaction between NOM and U–KCl, while the precipitation of U–K-bearing crystalline solids is evident after 24 h of reaction. Carbonation reactions in the presence of U(VI) have been previously observed[66] within these time scales, and the surface of the POM could facilitate heterogeneous nucleation of U–K-bearing crystals as the reaction time progresses from 0.5 to 24 h. Our results are unique given that other studies only focused on the adsorption of U onto organic material.[32] However, other investigations have shown that other metal ions adsorbed to POM can lead to the growth of metal–NOM crystalline phases.[68] Also, it has been reported that the growth of new solid phases typically involves metastable amorphous nano-particle or cluster compounds generated during the initial stages of heterogeneous precipitation reactions.[69]

After an initial decrease, the U concentration increased after 24 h in the U–KCl-NOM solution at pH 2 and pH 4 due to the following: (1) U desorption reactions or (2) the dissolution of U-bearing solids that may have precipitated during the reaction with NOM. Previous work investigating the adsorption of U onto natural sediments reported the temporary adsorption of U–NOM complexes.[70]

Our observations show that at pH 7, U remains in solution in the presence of NOM. Aqueous complexation of U-DOM enhances the solubility of U at circumneutral pH. Other studies have shown the adsorption of U onto NOM increases with pH below pH 7. Conversely, U adsorption decreases at pH 7. Another consideration is that our experiments were conducted under ambient conditions and it is possible that there was equilibrium with the atmosphere, in which the total dissolved inorganic carbon would be approximately 10^{-4} M predominantly present as bicarbonate. Thus, complexation between U and dissolved inorganic carbon is another possible reaction that could affect the system.

Environmental Implications.

We observed the "rebound" in dissolved U(VI) concentrations between 0.5 and 24 h and the precipitation of nanocrystalline U(VI) phases in the presence of NOM at pH 4. These findings have implications for transport modeling in natural and engineered systems at low pH. The observed "rebound" occurs in the typical contact time of treatment processes such as ion exchange and precipitation processes. NOM-facilitated precipitation of low solubility, nanocrystalline U-bearing solids at pH 4 could have long-term consequences for

the mobility of U(VI) in the environment compared to labile adsorbed U(VI) species. Future research should investigate the kinetics of adsorption, surface precipitation, dissolution, and desorption reactions of U with POM under low pH conditions relevant to acid mine drainage.

Supplementary Material

Refer to Web version on PubMed Central for supplementary material.

ACKNOWLEDGMENTS

REFERENCES

(1). Hettiarachchi E; Paul S; Cadol D; Frey B; Rubasinghege G Mineralogy controlled dissolution of uranium from airborne dust in simulated lung fluids (SLFs) and possible health implications. Environ. Sci. Technol. Lett 2018, 6, 62–67. [PubMed: 30775400]

(2). Wilson A; Velasco CA; Herbert GW; Lucas SN; Sanchez BN; Cerrato JM; Spilde M; Li Q-Z; Campen MJ; Zychowski KE Mine-site derived particulate matter exposure exacerbates neurological and pulmonary inflammatory outcomes in an auto-immune mouse model. J. Toxicol. Environ. Health, Part A 2021, 84, 503–517.

(3). El Hayek E; Medina S; Guo J; Noureddine A; Zychowski KE; Hunter R; Velasco CA; Wiesse M; Maestas-Olguin A; Brinker CJ; Brearley A; Spilde M; Howard T; Lauer FT; Herbert G; Ali AM; Burchiel S; Campen MJ; Cerrato JM Uptake and toxicity of respirable carbon-rich uranium-bearing particles: insights into the role of particulates in uranium toxicity. Environ. Sci. Technol 2021, 55, 9949–9957. [PubMed: 34235927]

(4). Cumberland SA; Etschmann B; Brugger J; Douglas G; Evans K; Fisher L; Kappen P; Moreau JW Characterization of uranium redox state in organic-rich Eocene sediments. Chemosphere 2018, 194, 602–613. [PubMed: 29241135]

(5). Velasco CA; Artyushkova K; Ali A-MS; Osburn CL; Gonzalez-Estrella J; Lezama-Pacheco JS; Cabaniss SE; Cerrato JM Organic functional group chemistry in mineralized deposits containing U(IV) and U(VI) from the Jackpile Mine in New Mexico. Environ. Sci. Technol 2019, 53, 5758–5767. [PubMed: 30998849]

(6). Bhattacharyya A; Campbell KM; Kelly SD; Roebbert Y; Weyer S; Bernier-Latmani R; Borch T Biogenic non-crystalline U(IV) revealed as major component in uranium ore deposits. Nat. Commun 2017, 8, 15538. [PubMed: 28569759]

(7). Blake JM; De Vore CL; Avasarala S; Ali A-M; Roldan C; Bowers F; Spilde MN; Artyushkova K; Kirk MF; Peterson E; Rodriguez-Freire L; Cerrato JM Uranium mobility and accumulation along the Rio Paguate, Jackpile Mine in Laguna Pueblo, NM. Environ. Sci.: Processes Impacts 2017, 19, 605–621.

(8). El Hayek E; Torres C; Rodriguez-Freire L; Blake JM; De Vore CL; Brearley AJ; Spilde MN; Cabaniss S; Ali A-MS; Cerrato JM Effect of calcium on the bioavailability of dissolved

uranium(VI) in plant roots under circumneutral pH. Environ. Sci. Technol 2018, 52, 13089–13098. [PubMed: 30412391]

(9). Trueman BF; Anaviapik-Soucie T; L'Hérault V; Gagnon GA Characterizing colloidal metals in drinking water by field flow fractionation. Environ. Sci. Water Resour 2019, 5, 2202–2209.

(10). Aiken GR; McKnight DM; Wershaw RL; MacCarthy P Humic Substances in Soil, Sediment, and Water. Soil Sci 1986, 142, 323.

(11). Suffet IH; MacCarthy P Aquatic Humic Substances: Influence on Fate and Treatment of Pollutants; American Chemical Society: Washington, DC, 1988.

(12). Volkov IV; Polyakov EV Interaction of humic acids with microelements/radionuclides in sorption systems. Radiochemistry 2020, 62, 141–160.

(13). Lan T; Liao J; Yang Y; Chai Z; Liu N; Wang D Competition/cooperation between humic acid and graphene oxide in uranyl adsorption implicated by molecular dynamics simulations. Environ. Sci. Technol 2019, 53, 5102–5110. [PubMed: 30945863]

(14). Lan T; Wang H; Liao J; Yang Y; Chai Z; Liu N; Wang D Dynamics of humic acid and its interaction with uranyl in the presence of hydrophobic surface implicated by molecular dynamics simulations. Environ. Sci. Technol 2016, 50, 11121–11128. [PubMed: 27666876]

(15). Weng L; Temminghoff EJM; Lofts S; Tipping E; Van Riemsdijk WH Complexation with dissolved organic matter and solubility control of heavy metals in a sandy soil. Environ. Sci. Technol 2002, 36, 4804–4810. [PubMed: 12487303]

(16). Li D; Kaplan DI; Chang H-S; Seaman JC; Jaffé PR; Koster van Groos P; Scheckel KG; Segre CU; Chen N; Jiang D-T; Newville M; Lanzirotti A Spectroscopic evidence of uranium immobilization in acidic wetlands by natural organic matter and plant roots. Environ. Sci. Technol 2015, 49, 2823–2832. [PubMed: 25634067]

(17). Bordelet G; Beaucaire C; Phrommavanh V; Descostes M Chemical reactivity of natural peat towards U and Ra. Chemosphere 2018, 202, 651–660. [PubMed: 29602097]

(18). Omar HA; Aziz M; Shakir K Adsorption of U(VI) from dilute aqueous solutions onto peat moss. Radiochim. Acta 2007, 95, 17–24.

(19). Bone SE; Dynes JJ; Cliff J; Bargar JR Uranium(IV) adsorption by natural organic matter in anoxic sediments. Proc. Natl. Acad. Sci. U. S. A 2017, 114, 711. [PubMed: 28069941]

(20). Du L; Li S; Li X; Wang P; Huang Z; Tan Z; Liu C; Liao J; Liu N Effect of humic acid on uranium(VI) retention and transport through quartz columns with varying pH and anion type. J. Environ. Radioact 2017, 177, 142–150. [PubMed: 28667877]

(21). Cumberland SA; Wilson SA; Etschmann B; Kappen P; Howard D; Paterson D; Brugger J Rapid immobilisation of U(VI) by Eucalyptus bark: Adsorption without reduction. Appl. Geochem 2018, 96, 1–10.

(22). Pan Z; Bártová B; LaGrange T; Butorin SM; Hyatt NC; Stennett MC; Kvashnina KO; Bernier-Latmani R Nanoscale mechanism of UO_2 formation through uranium reduction by magnetite. Nat. Commun 2020, 11, 4001. [PubMed: 32778661]

(23). Wang Y; Frutschi M; Suvorova E; Phrommavanh V; Descostes M; Osman AAA; Geipel G; Bernier-Latmani R Mobile uranium(IV)-bearing colloids in a mining-impacted wetland. Nat. Commun 2013, 4, 2942. [PubMed: 24346245]

(24). Cumberland SA; Douglas G; Grice K; Moreau JW Uranium mobility in organic matter-rich sediments: A review of geological and geochemical processes. Earth Sci. Rev 2016, 159, 160–185.

(25). Ravel B; Newville M ATHENA,ARTEMIS,HEPHAESTUS: data analysis for X-ray absorption spectroscopy usingIFEFFIT. J. Synchrotron Radiat 2005, 12, 537–541. [PubMed: 15968136]

(26). Tinnacher RM; Nico PS; Davis JA; Honeyman BD Effects of fulvic acid on Uranium(VI) sorption kinetics. Environ. Sci. Technol 2013, 47, 6214–6222. [PubMed: 23550952]

(27). Ahmad A; Rutten S; Eikelboom M; de Waal L; Bruning H; Bhattacharya P; van der Wal A Impact of phosphate, silicate and natural organic matter on the size of Fe(III) precipitates and arsenate co-precipitation efficiency in calcium containing water. Sep. Purif. Technol 2020, 235, 116117.

(28). Russell CG; Lawler DF; Speitel GE; Katz LE Effect of softening precipitate composition and surface characteristics on natural organic matter adsorption. Environ. Sci. Technol 2009, 43, 7837–7842. [PubMed: 19921902]

(29). Gorman-Lewis D; Burns PC; Fein JB Review of uranyl mineral solubility measurements. J. Chem. Thermodyn 2008, 40, 335–352.

(30). Gorman-Lewis D; Fein JB; Burns PC; Szymanowski JES; Converse J Solubility measurements of the uranyl oxide hydrate phases metaschoepite, compreignacite, Na-compreignacite, becquerelite, and clarkeite. J. Chem. Thermodyn 2008, 40, 980–990.

(31). Lenhart JJ; Cabaniss SE; MacCarthy P; Honeyman BD Uranium(VI) complexation with citric, humic and fulvic acids. Radiochim. Acta 2000, 88, 345–354.

(32). Lenhart JJ; Honeyman BD Uranium(VI) sorption to hematite in the presence of humic acid. Geochim. Cosmochim. Acta 1999, 63, 2891–2901.

(33). Bargar JR; Reitmeyer R; Lenhart JJ; Davis JA Characterization of U(VI)-carbonato ternary complexes on hematite: EXAFS and electrophoretic mobility measurements. Geochim. Cosmochim. Acta 2000, 64, 2737–2749.

(34). Giammar DE; Hering JG Time Scales for Sorption–Desorption and Surface Precipitation of Uranyl on Goethite. Environ. Sci. Technol 2001, 35, 3332–3337. [PubMed: 11529573]

(35). Waite TD; Davis JA; Payne TE; Waychunas GA; Xu N Uranium(VI) adsorption to ferrihydrite: Application of a surface complexation model. Geochim. Cosmochim. Acta 1994, 58, 5465–5478.

(36). Bednar AJ; Medina VF; Ulmer-Scholle DS; Frey BA; Johnson BL; Brostoff WN; Larson SL Effects of organic matter on the distribution of uranium in soil and plant matrices. Chemosphere 2007, 70, 237–247. [PubMed: 17709130]

(37). Anderson LE; Trueman BF; Dunnington DW; Gagnon GA Relative importance of organic- and iron-based colloids in six Nova Scotian lakes. npj Clean Water 2021, 4, 26.

(38). Dublet G; Lezama Pacheco J; Bargar JR; Fendorf S; Kumar N; Lowry GV; Brown GE Partitioning of uranyl between ferrihydrite and humic substances at acidic and circum-neutral pH. Geochim. Cosmochim. Acta 2017, 215, 122–140.

(39). Stetten L; Blanchart P; Mangeret A; Lefebvre P; Le Pape P; Brest J; Merrot P; Julien A; Proux O; Webb SM; Bargar JR; Cazala C; Morin G Redox fluctuations and organic complexation govern uranium redistribution from U(IV)-Phosphate Minerals in a mining-polluted wetland soil, Brittany, France. Environ. Sci. Technol 2018, 52, 13099–13109. [PubMed: 30339761]

(40). Zsolnay A; Baigar E; Jimenez M; Steinweg B; Saccomandi F Differentiating with fluorescence spectroscopy the sources of dissolved organic matter in soils subjected to drying. Chemosphere 1999, 38, 45–50. [PubMed: 10903090]

(41). K epelová A; Sachs S; Bernhard G Uranium(VI) sorption onto kaolinite in the presence and absence of humic acid. Radiochim. Acta 2006, 94, 825–833.

(42). Tomaži B; Branica M Precipitation and hydrolysis of uranium(VI) in aqueous solutions—VII: Boundary conditions for precipitation from solutions of $UO_2(NO_3)_2$-KOH-K, Ba, La and Eu nitrate. J. Inorg. Nucl. Chem 1972, 34, 1319–1332.

(43). Tomaži B; Samaržija M; Branica M Precipitation and hydrolysis of uranium(VI) in aqueous solutions-VI. J. Inorg. Nucl. Chem 1969, 31, 1771.

(44). Sowder AG; Clark SB; Fjeld RA The effect of silica and phosphate on the transformation of schoepite to becquerelite and other uranyl phases. Radiochim. Acta 1996, 74, 45–50.

(45). Kim K-W; Kim Y-H; Lee S-Y; Lee J-W; Joe K-S; Lee E-H; Kim J-S; Song K; Song K-C Precipitation Characteristics of Uranyl Ions at Different pHs Depending on the presence of carbonate ions and hydrogen peroxide. Environ. Sci. Technol 2009, 43, 2355–2361. [PubMed: 19452886]

(46). Giammar DE; Hering JG Influence of dissolved sodium and cesium on uranyl oxide hydrate solubility. Environ. Sci. Technol 2004, 38, 171–179. [PubMed: 14740733]

(47). Gang M-J; Han B-E; Hahn P-S Precipitation and adsorption of uranium(VI) under various aqueous conditions. Environ. Eng. Res 2002, 7, 149–157.

(48). Kanematsu M; Perdrial N; Um W; Chorover J; O'Day PA Influence of phosphate and silica on U(VI) precipitation from acidic and neutralized wastewaters. Environ. Sci. Technol 2014, 48, 6097–6106. [PubMed: 24754743]

(49). Denecke MA; Pompe S; Reich T; Moll H; Bubner M Measurements of the structural parameters for the interaction of uranium(VI) with natural and synthetic humic acids using EXAFS. Radiochim. Acta 1997, 79, 151–160.

(50). Regenspurg S; Margot-Roquier C; Harfouche M; Froidevaux P; Steinmann P; Junier P; Bernier-Latmani R Speciation of naturally-accumulated uranium in an organic-rich soil of an alpine region (Switzerland). Geochim. Cosmochim. Acta 2010, 74, 2082–2098.

(51). Mikutta C; Langner P; Bargar JR; Kretzschmar R Tetra- and hexavalent uranium forms bidentate-mononuclear complexes with particulate organic matter in a naturally uranium-enriched peatland. Environ. Sci. Technol 2016, 50, 10465–10475. [PubMed: 27635434]

(52). Schmeide K; Sachs S; Bubner M; Reich T; Heise KH; Bernhard G Interaction of uranium(VI) with various modified and unmodified natural and synthetic humic substances studied by EXAFS and FTIR spectroscopy. Inorg. Chim. Acta 2003, 351, 133–140.

(53). Kelly SD; Kemner KM; Fein JB; Fowle DA; Boyanov MI; Bunker BA; Yee N X-ray absorption fine structure determination of pH-dependent U-bacterial cell wall interactions. Geochim. Cosmochim. Acta 2002, 66, 3855–3871.

(54). Merroun ML; Raff J; Rossberg A; Hennig C; Reich T; Selenska-Pobell S Complexation of Uranium by Cells and S-Layer Sheets ofBacillus sphaericus JG-A12. Appl. Environ. Microbiol 2005, 71, 5532–5543. [PubMed: 16151146]

(55). Dunham-Cheatham S; Rui X; Bunker B; Menguy N; Hellmann R; Fein J The effects of non-metabolizing bacterial cells on the precipitation of U, Pb and Ca phosphates. Geochim. Cosmochim. Acta 2011, 75, 2828–2847.

(56). Seder-Colomina M; Morin G; Brest J; Ona-Nguema G; Gordien N; Pernelle J-J; Banerjee D; Mathon O; Esposito G; van Hullebusch ED Uranium(VI) scavenging by amorphous iron phosphate encrusting Sphaerotilus natans filaments. Environ. Sci. Technol 2015, 49, 14065–14075. [PubMed: 26544528]

(57). Brandes JA; Wirick S; Jacobsen C Carbon K-edge spectra of carbonate minerals. J. Synchrotron Radiat 2010, 17, 676–682. [PubMed: 20724789]

(58). Charushnikova IA; Grigor'ev MS; Krot NN Synthesis and crystal structure of new U(VI) and Np(VI) benzoates, $K_{11}(AnO_2)_{23}(OOCC_6H_5)_{57}(H_2O)_{18+x}$. Radiochemistry 2010, 52, 138–144.

(59). Kubatko K-A; Helean KB; Navrotsky A; Burns PC Thermodynamics of uranyl minerals: Enthalpies of formation of rutherfordine, UO_2CO_3, andersonite, $Na_2CaUO_2(CO_3)_{(3)}(H_2O)_{(5)}$, and grimselite, $K_3NaUO_2(CO_3)_{(3)}H_2O$. Am. Mineral 2005, 90, 1284–1290.

(60). O'Brien TJ; Williams PA The aqueous chemistry of uranium minerals. 4. Schröckingerite, grimselite, and related alkali uranyl carbonates. Mineral. Mag 1983, 47, 69–73.

(61). Goldstone JV; Pullin MJ; Bertilsson S; Voelker BM Reactions of Hydroxyl Radical with Humic Substances: Bleaching, Mineralization, and Production of Bioavailable Carbon Substrates. Environ. Sci. Technol 2002, 36, 364–372. [PubMed: 11871550]

(62). Gao H; Zepp RG Factors influencing photoreactions of dissolved organic matter in a coastal river of the Southeastern United States. Environ. Sci. Technol 1998, 32, 2940–2946.

(63). Liao Z-L; Li G-D; Bi M-H; Chen J-S Preparation, Structures, and Photocatalytic Properties of Three New Uranyl–Organic Assembly Compounds. Inorg. Chem 2008, 47, 4844–4853. [PubMed: 18447330]

(64). Thangavelu SG; Cahill CL Uranyl-promoted peroxide generation: synthesis and characterization of three uranyl peroxo $[(UO_2)_2(O_2)]$ complexes. Inorg. Chem 2015, 54, 4208–4221. [PubMed: 25875867]

(65). Kravchuk DV; Forbes TZ In situ generation of organic peroxide to create a nanotubular uranyl peroxide phosphate. Angew. Chem., Int. Ed 2019, 58, 18429–18433.

(66). Kravchuk DV; Dahlen NN; Kruse SJ; Malliakas CD; Shand PM; Forbes TZ Isolation and reactivity of uranyl superoxide. Angew. Chem., Int. Ed 2021, 60, 15041.

(67). Blanes Díaz A; Kravchuk DV; Peroutka AA; Cole E; Basile MC; Forbes TZ Photoinduced transformation of uranyl nitrate crown ether compounds. Eur. J. Inorg. Chem 2021, 2021, 166–176.

(68). Gavrilescu M; Pavel LV; Cretescu I Characterization and remediation of soils contaminated with uranium. J. Hazard. Mater 2009, 163, 475–510. [PubMed: 18771850]

(69). Aiken GR; Hsu-Kim H; Ryan JN Influence of dissolved organic matter on the environmental fate of metals, nanoparticles, and colloids. Environ. Sci. Technol 2011, 45, 3196–3201. [PubMed: 21405118]

(70). Izquierdo M; Young SD; Bailey EH; Crout NMJ; Lofts S; Chenery SR; Shaw G Kinetics of uranium(VI) lability and solubility in aerobic soils. Chemosphere 2020, 258, 127246. [PubMed: 32535442]
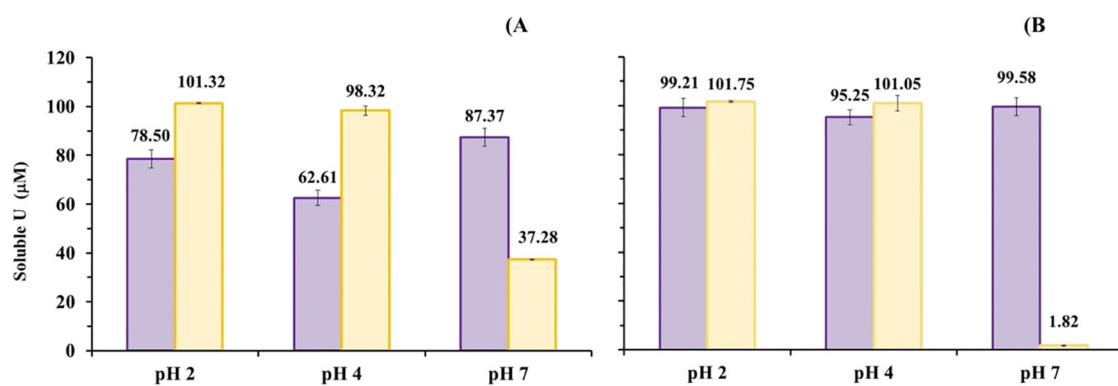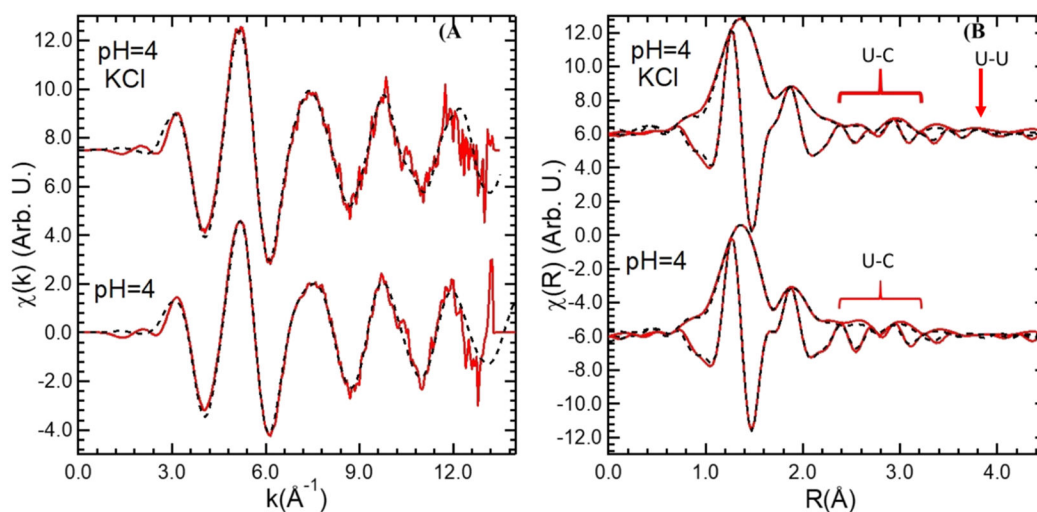
Sampling	Soluble U (µM)					
Time	**pH 2**		**pH 4**		**pH 7**	
	U-KCl-NOM	U-KCl	U-KCl-NOM	U-KCl	U-KCl-NOM	U-KCl
After 0.5 hr.	78.5±10.8	101.3±5.3	62.6±19.3	98.3±0.5	87.4±3.3	37.3±13.1
After 24 hr.	99.2±3.7	101.7±1.8	95.3±3.1	101.1±1.8	99.6±3.7	1.8±0.7

Figure 1.
Soluble U concentration in batch experiments containing NOM, U and KCl (purple), and U control experiment (yellow) at (A) 0.5, (B) 24 h, and (C) soluble U concentration summary results. Initial concentrations used are 200 mg L^{-1} NOM and 100 μM-UO$_2$(NO$_3$)$_2$ in 0.01 M KCl.

Correlations		U-NOM	U-KCl-NOM
	N	2*	
U-O1	R(Å)	1.78(1)	1.78(1)
	$\sigma^2(\text{Å}^2)$	0.0028(1)	0.0025(2)
	N	2.9(5)	3.3(2)
U-O2	R(Å)	2.27(4)	2.26(2)
	$\sigma^2(\text{Å}^2)$	0.0098(24)	0.0057(1)
	N	4.1(5)	3.7(2)
U-O21	R(Å)	2.43(3)	2.43(2)
	$\sigma^2(\text{Å}^2)$	0.0098(24)	0.0057(1)
	N	1.4(4)	0.9(4)
U-C1	R(Å)	2.90(2)	2.90(3)
	$\sigma^2(\text{Å}^2)$	0.004*	
	N	2.6(8)	3.0(8)
U-C2	R(Å)	3.43(4)	3.44(3)
	$\sigma^2(\text{Å}^2)$	0.010*	
	N		0.5(3)
U-U1	R(Å)		3.94(3)
	$\sigma^2(\text{Å}^2)$		0.0053

*Denotes a fixed value derived from model compounds

Figure 2.
XAS of solids collected from U–KCl-NOM and U-NOM batch experiments at pH 4 after 24 h reaction. (A) U L$_{\text{III}}$-edge EXAFS, (B) EXAFS Fourier transform, and shell-by-shell fits indicate the presence of U likely bound to organic functional groups from POM through adsorption and U–U due to the presence of crystalline solid phases only in sample from the U–KCl-NOM experiment. (C) Result table for shell-by-shell fits of the EXAFS signal.
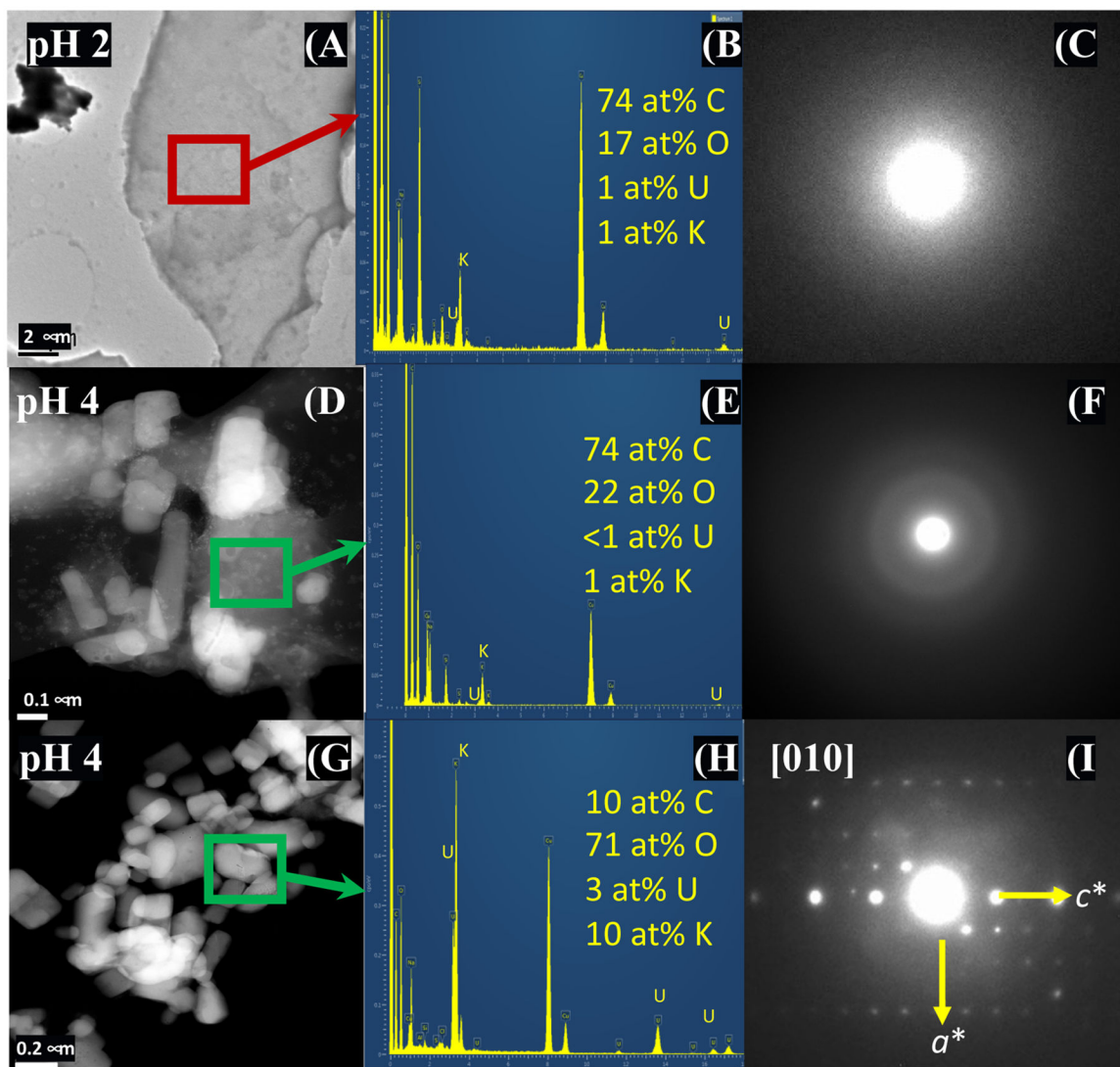
Figure 3.
BFTEM and DR-STEM images, EDS spectra, and SAED patterns for solids collected from batch reactions of U–KCl-NOM after 24 at pH 2 (A–C) and pH 4 (D–I). TEM image and SAED pattern (A,C) show the adsorption of U onto amorphous POM at pH 2, indicated by the presence of a distinct U X-ray peak in the EDS spectrum (B). EDS indicates low concentrations of U adsorbed onto POM (E), and SAED shows diffuse diffraction rings characteristic of an amorphous phase (F) at pH 4 that contains lower concentrations of U than at pH 2. Crystallites of U–K–Na-bearing solids that were identified at pH 4 (G,H) and slightly tilted SAED pattern that is consistent with the [010] zone axis of grimselite (I).
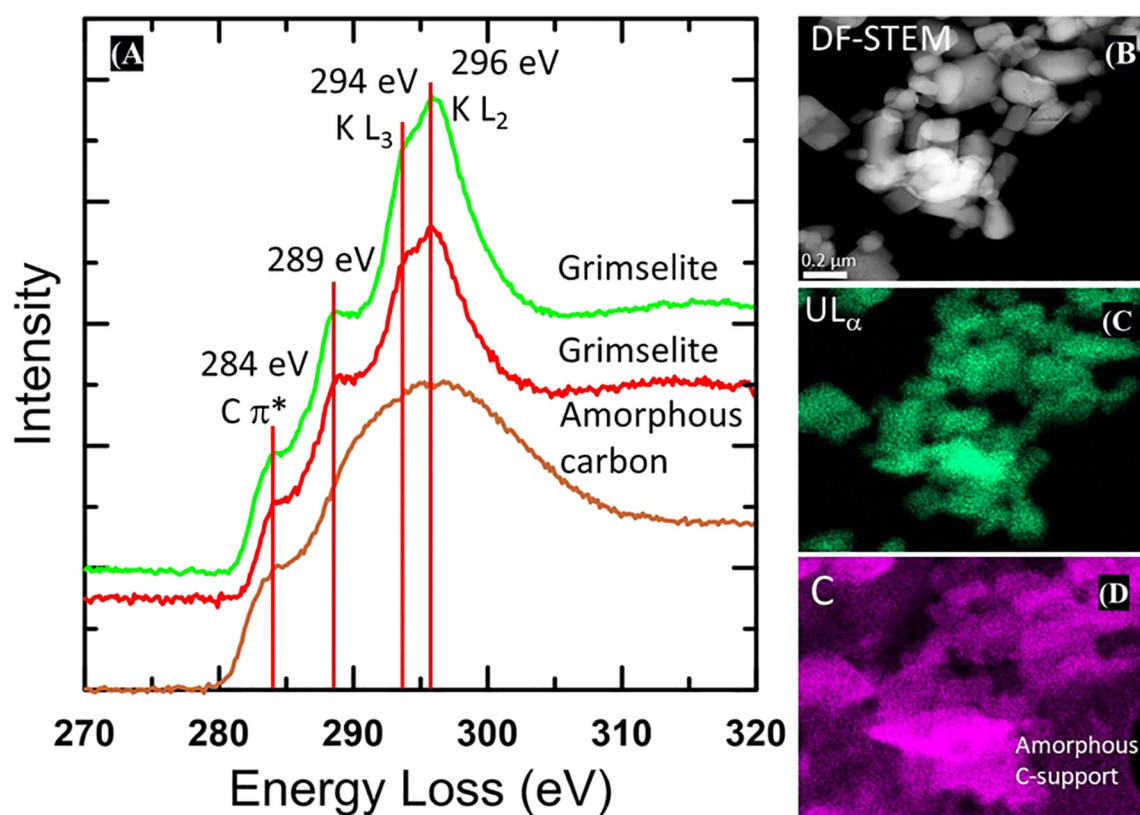
Figure 4.
EELS from solid collected after the reaction of U–KCl-NOM at pH 4 for 24 h. (A) DF-STEM image (B) and STEM–EDS X-ray maps (C,D). Two EEL spectra for grimselite are for the crystalline U- and K-bearing solids, which have been identified as grimselite-based electron diffraction data (Figure 3) are shown in red and green showing the presence of the K L3 and L2 3 edges at 294 and 296 eV, respectively. A distinct shoulder is present on the lower energy side of the K edge at 289 eV, which could be attributable to either carbonate or carboxylic groups. The lower spectrum (brown) is from the amorphous holey carbon film support with a distinct 284 eV edge that can be assigned to the C π* peak. This feature is also apparent in the grimselite spectra because the crystallites occur directly on the holey carbon film support. The 289 eV feature is not present in the amorphous carbon substrate. Right hand images show a DF-STEM image of the crystallites and X-ray maps of U and C, demonstrating that the crystallites contain C associated with U. An X-ray signal from the amorphous holey carbon film is clearly apparent in the lower right and upper left of the carbon X-ray map.